Journal of Applied Fluid Mechanics, Vol. 13, No. 6, pp. 1781-1793, 2020.
Available online at www.jafmonline.net, ISSN 1735-3572, EISSN 1735-3645.
DOI: 10.47176/jafm.13.06.31370

Continuous Wavelet Transform Analysis of Turbulent Wall Jet Evolving Through a Backward Facing Step

K. Zaibak[1,2†], N. Nait Bouda[3], S. Biskri[1], F. Mekideche-Chafa[1] and Y. Chibani[4]

[1] *Theoretical Physics Laboratory, Faculty of Physics, University of Sciences and Technology Houari Boumediene, USTHB, P. B. 32, El-Alia 16111, Algiers, Algeria*
[2] *Laboratory of Particle and Statistical Physics, Ecole Normale Supèrieure-Kouba, P. B. 92, 16050, Vieux Kouba, Algiers, Algeria*
[3] *Laboratory of Theoretical and Applied Fluid Mechanics, Faculty of Physics, University of Sciences and Technology Houari Boumediene, USTHB, P. B. 32, El-Alia 16111, Algiers, Algeria*
[4] *Communicating and Intelligent System Engineering Laboratory, Faculty of Electronics and Computer Science, University of Sciences and Technology Houari Boumediene, USTHB, P. B. 32, El-Alia, 16111, Algiers, Algeria*

†*Corresponding Author Email: kenzaibak4@gmail.com*

(Received January 20, 2020; accepted April 17, 2020)

ABSTRACT

A continuous wavelet transform (CWT) is used to detect the most important scales governing the dynamics of a turbulent wall jet flow that evolves through a backward facing step. Our particular interest is the region downstream of the step. The fluctuating velocity signals obtained experimentally by a laser Doppler anemometer at different heights from the wall are first analyzed in Fourier space by performing the density energy spectra (PSD). In the recirculation zone, we noticed that the flow loses its equilibrium when we approach the wall. This is obviously due to the complex nature of flow dynamics which exhibits a complex structure with various scales. Then, we applied the CWT with two wavelet functions: the eighth derivative of a Gaussian which is selected on the basis of the wavelet entropy measures and a Morlet wavelet. The first one is used to locate the more energetic structures and the second to detect the dominant frequencies of the high energy structures. It turns out that, in the external zone characterized by the presence of intermittent eddies; most of the energy is concentrated in the large scale structures. In the shear layer, different scales of structures are observed. We can also observe the physical phenomena such as extension or breakup of structures. In addition, the relative wavelet energy is applied to give the energy distribution at each scale. On the other hand, the Morlet wavelet is used in order to monitor the dragging of large structures characterized by a low frequency (large scale) originating from the wall-jet's external region towards the reattachment region. It is shown that the energy of these eddy structures decreases along their dragging.

Keywords: Continuous wavelet transform; Morlet wavelet; The eighth derivative of a Gaussian wavelet; Turbulent flow; Wall jet; Wavelet entropy.

NOMENCLATURE

b	nozzle height
CWT	Continuous Wavelet Transform
FT	Fourier Transform
h	step height
l	nozzle width
L_1	upstream flat plate length
L_2	downstream flat plate length
RWE	Relative Wavelet Energy
u	streamwise velocity fluctuation
U_0	maximum streamwise velocity at x = -15h
x, y, z	streamwise, Vertical and Spanwise directions

1. INTRODUCTION

The wavelet transform is a mathematical method that is based on group theory and square integrable group representations (Bernier and Taylor 1996). This method decomposes a given signal into both space (time) and scale (frequency) by convoluting it with a given analyzing function called wavelet, which is a well localized function in space (time).

The analyzing wavelet can be dilated or contracted at will, which means that the wavelet transform can be performed locally in both time and frequency space on the signal. For this reason, this method is well suited for the study of non-stationary, non-periodic, intermittent and transient signals.

The wavelet transform may take two forms, the continuous and the discrete wavelet transforms (Daubechies *et al.* 1986). The discrete wavelet transform (DWT) can decompose data into wavelet coefficients of different scales that are independent and orthogonal to each other. This transform can be used for signal reconstruction and data compression. The use of the continuous wavelet transform (CWT) permits a continuous and redundant unfolding in terms of scale and time thanks to the freedom in the choice of the wavelet function. Therefore this transform is mostly used for identifying localized regions of energy concentration and feature detection in arbitrary signals.

Applications of the wavelet transform occur in many different fields (Meringolo *et al.* 2017; Abid and Kaffel 2018; Fernández-Macho 2018; Beibei *et al.* 2018; Szadkowski 2014; Belayadi *et al.* 2017), particularly in the analysis of turbulent flows, where the instantaneous signals exhibit non-stationary and non-linear features. The wavelet transform is a powerful tool that helps bring together two different descriptions of turbulent flows: the first one is the Fourier spectral analysis that describes the energy cascade between the different frequency scales and the second is the presence of eddy structures in the physical space. Indeed, the wavelet transform decomposition of the fluctuating velocity signals allows a frequency-time representation of the eddy structures present in a turbulent flow.

The application of the wavelet transform method in order to study turbulence in fluids was introduced by Farge (1992). She used the Morlet wavelet to analyze two-dimensional homogeneous turbulent flows obtained from numerical simulations. In this study, it was found that, during the flow evolution, the small scales of the vorticity field become increasingly localized in physical space. Zheng *et al.* (2016) used the continuous wavelet transform to analyze multiscale turbulent structures of the wake flow. Lysenko *et al.* (2014) performed the continuous wavelet transform on transverse velocity time series extracted in the wake of a circular cylinder. This analysis allowed to quantify precisely the separated shear-layer instabilities. Seena and Jin Sung (2011) applied the wavelet transform to both the temporal signal and spatial fields for extracting structures from the oscillating shear layer in turbulent cavity flows. Xia *et al.* (2009) applied the discrete wavelet transform using a Daubechies wavelet with more vanishing moments for studying the energy transfer of multiscale structures in a turbulent boundary layer. They found that the physical phenomena such as deformation or breakup of eddies are related to the vertical position in the boundary layer, and the energy-containing eddies exist in a multiscale form. Lately, wavelet analysis was used in the study of a jet flow. Li *et al.* (1999) applied orthogonal wavelets to the turbulent images for the identification of the multiscale turbulent structures. Yao *et al.* (2015) proposed a multiscale analysis method based on the discrete wavelet transform using a Daubechies wavelet with order equal to 6 to gain deeper insight into the multiscale turbulent structures and to extract the most essential scales governing the development of the turbulent flow structures of the jet impinging on a flat surface. Li (1997) applied the wavelet autocorrelation using the Morlet wavelet to analyze the eddy structure of a turbulent shear flow. He found that a periodic large eddy motion contains the periodical small eddy motions. Lim *et al.* (2008) performed the continuous wavelet transform using the Morlet wavelet to study the coherent structures in jet column region of a sharp edged orifice plane jet. It is found that the eddy breakdown at downstream, which successive branching of the vortical structures produces multifractal structures of eddies.

A turbulent flow is characterized by eddy structures at various scales. Fourier transform can decompose a velocity field into waves of different wavelengths; each wave is associated with a single Fourier coefficient. However, an eddy of wavelength $\lambda = 2\pi/k$, containing an energy of wave number k in spectrum, which is defined in a physical space as a declined wave with limited scale is associated with many Fourier coefficients and the phase relations among them, as Tennekes and Lumley (1972) pointed out. Fourier transform cannot distinguish between waves and eddies. Therefore, we need other sophisticated transform when we want to decompose a velocity field into eddies rather than waves. The CWT, which can analyze the local characteristics of a signal, is well suitable to detect the eddy structures present in turbulent flow. Liu and Jiang (2004) have shown that the wavelet coefficient structure function is similar with the locally averaged velocity structure function rather than the classical velocity structure function used by Kolmogorov.

In the present work, the continuous wavelet transform is used in order to detect and extract different dynamical behaviors present in a turbulent wall jet evolving through a backward facing step.

The wall jet exhibits an important characteristic, namely, the interaction between the near-wall region, which has a boundary layer behavior, and a free shear flow that develops in the separating line at the outlet of the jet's nozzle (Eriksson *et al.* 1998). Thus the flow has two zones of turbulent production. The first is due to internal shear with small structures, and the second is related to the free shear with the fluid drive due to the large structures. The latter could presumably introduce a change in the flow dynamics through the backward facing step. From a statistical point of view, the wall jet could act on energy transfer between the turbulence scales by modifying the process of energy cascade of the large vortices towards the smallest vortices up to the dissipative scales. The spectral representation shows the existence of multiscale eddy structures, which modify the shape of the

spectrum with respect to the spectrum described by Kolmogorov's theory (Monin and Yaglom 1975; Pope 2000).

It should be noted that the flow configuration of turbulent wall jet over a backward facing step is encountered in many engineering process such as the cyclone filtration systems or separators, the alternator and electrical rotating machines that can be found in automobile engines and modern wind generators of the power production industry. In the environment it can be found, for example, in the formation of the snow avalanche. Therefore, the study of this configuration in laboratory is interesting for understanding and controlling the process of separation and reattachment.

A study of a turbulent wall jet over a backward facing step have been suggested by a some researchers including Jacob *et al*. (2001), Nait Bouda *et al*.(2008) and Thien and Harmand (2015). Jacob *et al*. (2001) performed aerodynamic and acoustic measurements of the turbulent wall jet over a backward facing step in an open channel. They found that the reattachment length was much shorter than that of the backward facing step flow in the plane channel. Thien and Harmand (2015) investigated the flow characteristics of a turbulent wall jet over a backward-facing step with the particle image velocimetry (PIV) and stereoscopic PIV measurements. They found that the mean reattachment length was much shorter than those from the backward-facing step in the channel. Nait Bouda *et al*. (2008) performed the numerical and experimental study of a turbulent wall jet over a backward facing step. They particularly found that the turbulent structures of the external zone of the wall jet have a significant influence on the development of the flow downstream of a backward facing step. Indeed, these large structures (small frequencies) penetrate inwards and generate large turbulent energy at the wall. Due to the introduced changes in the flow dynamics through the downward facing step, the reattachment length is reduced. The interpretation of the results is based on the presence of multiscale eddy structures in the turbulent flow downstream a backward facing step. In order to confirm this interpretation, we use the continuous wavelet transform (CWT) to monitor the formation and evolution of these structures. These analyzes are performed in all the different regions of the flow downstream the backward facing step (external region, shear layers, recirculation zone and in the region close to the wall). In addition, the relative wavelet energy (RWE) is employed as a quantitative measure for giving information about the signal energy distribution at various scales.

The remaining paper is structured as follows: Section 2 presents the geometrical configuration and reviews the measurement technique and the used interpolation technique for generating the required dataset. Section 3 is dedicated to evaluate the performance of the power spectral density (PSD) analysis performed on the streamwise velocity fluctuations measured at different heights from the wall downstream of the step. In the section 4, we describe the basic concept of the continuous wavelet transform (CWT). Then, we also define the Relative Wavelet Energy (RWE) and the Wavelet Entropy deduced from the CWT in order to capture the energy distribution at each scale and to select an appropriate wavelet mother respectively. Subsequently, Section 5 presents the performance of the CWT and the RWE performed on the velocity fluctuations that are measured by the PSD, and discussed. Finally, Section 6 concludes the paper by providing few remarks and suggestions.

2. EXPERIMENTAL SETUP AND MEASUREMENTS

2.1 Test Section

The geometrical configuration of a turbulent wall jet over a backward facing step is shown in Fig. 1 (Nait Bouda *et al*. 2008). The nozzle had a 40 mm high (b), the upstream flat plate measuring about 110 cm long (L_1) and 70 cm wide (l), and the downstream one of 100cm long (L_2) are connected through a step of 20mm height (h). The x, y and z coordinates represent respectively, the streamwise, vertical and spanwise directions. The experimental rig is limited by plane parallel walls made in plexiglass. The maximum velocity of the flow measured at the x/h = -15 cross section upstream the step is about U_0 = 5.8 m/s and the corresponding Reynolds number based on the step height is Re_h = 7600 with kinematic viscosity ν=1,56.10^{-5} m^2s^{-1}. Moreover, the intensity of the turbulence in the main flow is about 13%.

The seeding of the flow is provided by a smoke generator “Jem Techno Haze Performance” placed at the entrance of the wind tunnel.

The measurements of the three-dimensional velocity field of the flow are performed with a double measure in the (xoy) then (xoz) planes by a two components laser Doppler anemometer (LDA). The light beam is produced by an Argon-Ion laser of 2W power (details in Ref. Nait Bouda *et al*. 2008).

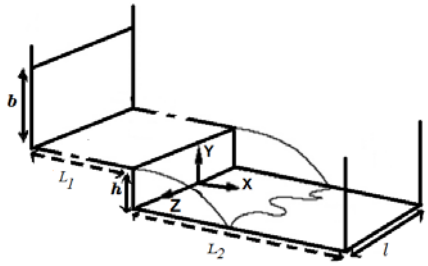

Fig. 1. Test geometry and nomenclature where: h=20mm, b=40mm, L_1=110cm, L_2=100cm, l=70cm (Nait Bouda *et al*. 2014**).**

In this paper, the analysis methods are applied on the streamwise velocity component signals.

2.2 The Overall Structure of Flow

The representation of the overall structure of the jet flow approaching a downward step is shown in Fig.

2 (Nait Bouda *et al.* 2008). The fully developed turbulent wall jet, upstream of the step (which means that when the local characteristic velocity and length scales are used, the dimensionless velocity profiles at different sections will tend to a similarity single profile), with an inner shear layer due to near wall velocity gradients and the free shear jet-like flow in the external region separates at the sharp step edge. Then, a shear layer, delimiting the recirculation zone by the lower boundary, develops from the edge of the step to reattach up further downstream. The relaxation region is one in which the flow ends up returning to the characteristics of the flow upstream of the step (Nait Bouda *et al.* 2008).

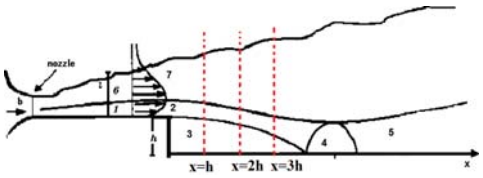

Fig 2. Schematic pattern of flow structure (Nait Bouda *et al.* 2008**) where: 1. Inner layer, 2. Shear layer, 3. Recirculation zone, 4. Reattachment region, 5. Relaxation region, 6 and 7. Free shear layers.**

2.3 Data and Background Analysis

It is important to note that the LDA signals of velocity are irregular in time, whereas the evaluation of spectral densities by the classical Fast Fourier Transform (FFT) methods requires regular sampling of the data. For this reason, we reconstructed the signal by a resampling technique, in accordance with the first-order interpolation criterion. In this case, the frequency is taken greater than or equal to 2.2 times the average acquisition rate d.r (for data rate) divided by 2π (Benedict 1998). In our case, the resampling frequency f_S equals 1000 Hz, the cut-off frequency f_c equals 100 Hz. Figure 3 shows an example of a sample time-series of the streamwise velocity component 'u' constructed by this method

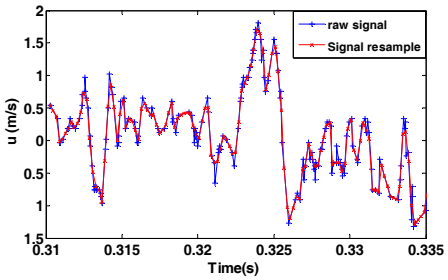

Fig. 3. Sample time-series constructed from the resampling method ($f_S = 10.f_c$).

In order to ensure a good statistical treatment, the minimal number of points must be larger than 2000 at all locations and then acquisition time is taken greater than 40s **(**Nait Bouda *et al.* 2008).

3. SPECTRAL ANALYSIS RESULTS

The power spectral density (PSD) is a commonly used tool to investigate the distribution of energy versus the frequency of the signal. It allows examining the energy cascade process in turbulent flows.

Figure 4 shows the PSD distribution of the streamwise velocity fluctuations which are obtained respectively at y= 2.5h, 1.15h, 0.85h and 0.35h along the measurement section x=2h. The straight line with slope -5/3 corresponds to the inertial zone of Kolmogorov (Monin and Yaglom 1975) in order to check the equilibrium state of the flow.

Close to the external region, at y= 2.5h, the energy spectrum of the velocity fluctuations shows that the maximum of energy is reached at low frequencies (large scales), and that this energy is transferred towards the high frequencies according to a slope that is very close to that predicted by the Kolmogorov theory in the inertial zone, which is proportional to -5/3(Fig. 4(a)).

In the shear zone, y = 1.15h, the energy begins to extend slightly toward higher frequencies compared to the y = 2.5h position. The slope of the straight line begins to deviate slightly from the extent of the inertial zone predicted by Kolmogorov. This behavior indicates that the flow begins to lose its equilibrium (Fig. 4(b)).

The energy spectra of the velocity fluctuations at y=0.85h (Fig 4(c)) and y=0.35h (Fig. 4(d)), which correspond to the recirculation zone and the region near wall respectively show that their slopes deviate completely from the extent of the inertial zone predicted by Kolmogorov. Therefore the flow is clearly out of equilibrium.

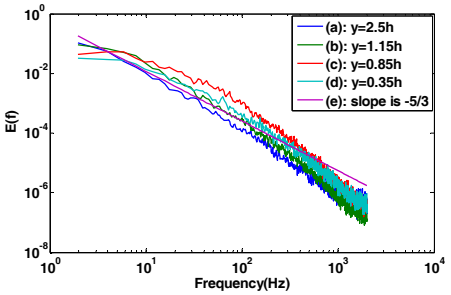

Fig. 4. PSD distribution of the streamwise velocity fluctuations at (a): y= 2.5h, (b): y= 1.15h, (c): y= 0.85h and (d): y= 0.35h along the measurement section x=2h.

It appears therefore that the equilibrium range is almost inexistent in the region where y/h< 1. This is probably due to the hybrid character of the flow, exhibiting a complex structure with the different scales, a characteristic resulting from the interaction of two different types of shear **(**Nait Bouda *et al.* 2008). Also, we can interpret these results geometrically, on the basis of the presence of multiscale eddy structures arising in the turbulent flow. A Fourier analysis is able to exhibit which

scales contribute to these transfers. However, this analysis cannot reflect the time evolution of the different eddies and it is unable also to extract the deformation or breakup of eddies.

4. THEORY OF CONTINUOUS WAVELET TRANSFORM

In contrast to the Fourier analysis, the CWT, which can analyze the local characteristics of a signal, is a very useful time frequency analytical tool to study the turbulence. Obviously, through this method, turbulence can be decomposed into various turbulent scales.

Let ψ (t) be a complex valued function. If ψ satisfies the admissibility condition (Grossmann and Morlet 1984; Qian 2002; Daubechies 1992; Addison 2002):

$$C_\psi = \int_0^{+\infty} \frac{|\hat{\psi}(\omega)|^2}{\omega} d\omega \prec \infty \tag{1}$$

where $\hat{\psi}(\omega)$ is the Fourier transform of $\psi(t)$,then $\psi(t)$ is called a mother wavelet.

The relation (1) implies that the wavelet must have a zero average, namely:

$$\int_{-\infty}^{+\infty} \psi(t)dt = \hat{\psi}(0) = 0, \tag{2}$$

which means it must be oscillating.

A wavelet $\psi(t)$ has n vanishing moments, if and only if, for all positive integers k < n, it satisfies:

$$\int_{-\infty}^{\infty} t^k \psi(t)dt = 0. \tag{3}$$

The mother wavelet ψ is dilated with a scale parameter a and is translated with the parameter b as follows:

$$\psi_{b,a}(t) = \frac{1}{\sqrt{a}} \psi\left(\frac{t-b}{a}\right), \quad b \epsilon \mathbb{R}, \quad a \epsilon \mathbb{R}^+ \tag{4}$$

where $\frac{1}{\sqrt{a}}$ is a normalization factor (Grossmann and Kronland Martinet 1982).

The relationship between the Fourier frequency f and the wavelet scale can be approximated by the following relation:

$$f = \frac{f_c \cdot f_s}{a}, \tag{5}$$

where f_c is the non-dimensional center frequency of the wavelet mother and f_s is the signal sampling rate. According to the relation in eq. (5), low frequency corresponds to large scale and vice versa.

The continuous wavelet transform of a finite energy signal S(t) with respect to the analyzing wavelet $\psi_{b,a}(t)$ is defined as their scalar product, namely:

$$W_S(b,a) = \langle S(t), \psi_{b,a} \rangle = \frac{1}{\sqrt{a}} \int_{-\infty}^{+\infty} \bar{\psi}\left(\frac{t-b}{a}\right) S(t)dt, \tag{6}$$

where $\langle\ \rangle$ is the scalar product in $L^2(\mathbb{R})$ ($L^2(\mathbb{R})$ denote the space of all square integrable functions on $\mathbb{R}$), $\bar{\psi}$ is the complex conjugate of ψ and W_S represents the coefficient of the decomposed signal S(t) at location b and scale a .

The continuous wavelet transform can be rewritten in term of Fourier transforms as:

$$W_S(b,a) = \sqrt{a} \int_{-\infty}^{\infty} \bar{\hat{\psi}}(a\omega)\hat{S}(\omega)e^{ib\omega} d\omega \tag{7}$$

where $\hat{S}(\omega)$ denotes the Fourier transform of S(t) and similarly for ψ .

With the help of Eq. (7), we can use in practice a fast Fourier transform (FFT) algorithm to speed up the computation of the wavelet transform (Watson and Addison 2002).

The global wavelet spectrum reflects the energy contained within the signal at a specific scale and is defined as:

$$E_W(a) = \frac{1}{2\pi C_\psi} \int_{-\infty}^{+\infty} |W_S(b,a)|^2 db. \tag{8}$$

Relative Wavelet Energy

The relative wavelet energy (RWE) gives information about the percentage of the energy at various scales to the total energy (Rosso *et al.* 2001). It can be defined as follows:

$$P_a = \frac{E_a}{E_T}, \tag{9}$$

where E_a is the energy component at each scale level and is given by the following relation:

$$E_a = \sum_b |W_S(b,a)|^2 \tag{10}$$

and the total energy of a CWT for all the scales can be obtained by:

$$E_T = \sum_a E_a. \tag{11}$$

4.2 Wavelet Entropy

The entropy is a quantitative measure of disorder in a system (Coifman and Wickerhauser 1992). In classical physics, it is proportional to the quantity of energy. The entropy is associated to the wavelet transform in order to estimate the degree of disorder of non-stationary signals.

The wavelet entropy can be defined as:

$$S = -\sum_a P_a . \ln(P_a). \tag{12}$$

The turbulent signals exhibit more disordered behavior since the turbulence happens at various

scales. Consequently, the wavelet entropy has a higher value which can be used as an effective quantitative measure to select the best mother wavelet.

4.3 Choice of mother wavelet

Many continuous wavelets have been proposed and designed for specific problems, such as the Gaussian, Mexican hat, and Morlet Wavelets. The choice of the appropriate wavelet mother depends on the type of information that we want to extract from the signal. These wavelets are described as follows:

4.3.1 The Gaussian wavelet

The Gaussian function is expressed as:

$$f(t) = e^{-\frac{t^2}{2}} \tag{13}$$

The n-th derivative of this function produces the Gaussian wavelet, and is given by the following expression:

$$\psi_n(t) = \frac{d^n f(t)}{dt^n}, \qquad n \succ 0 \tag{14}$$

Its Fourier transform is given by:

$$\hat{\psi}(\omega) = (i\omega)^n e^{-\frac{\omega^2}{2}} \tag{15}$$

These wavelets possess the property of having n vanishing moments. They are all admissible.

Figure 5 shows the plot of the 2nd, 5th and 8th derivatives of Gaussian wavelet (DGW). The second-order derivative of Gaussian is also known as the Mexican hat wavelet.

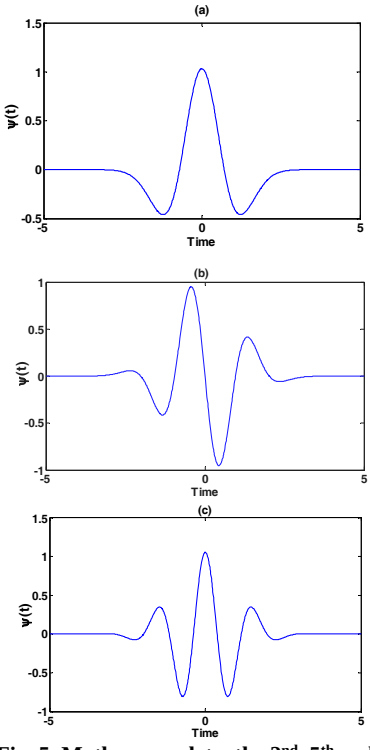

Fig. 5. Mother wavelets: the 2nd, 5th and 8th derivatives of Gaussian wavelet.

Since the region of the maximum value of the CWT can be interpreted as the scale of an eddy structure in turbulent flow (Li and Nozaki 1995), so it is advantageous to use as analyzing wavelet an even order derivative of the Gaussian function.

We propose to select the best even order derivative of the Gaussian wavelet for detecting the most important scales governing the dynamics of a turbulent based on qualitative and quantitative approaches:

4.3.1.1 Qualitative Approach

In order to select the best mother wavelet based on a qualitative approach, we apply the CWT to the velocity fluctuations at the position (x=2h, y=1.15h) located in the shear layer. Four mother wavelet functions (2nd, 6th, 8th and 12th derivatives of Gaussian) were selected for the purpose of comparison as shown in Fig. 6.

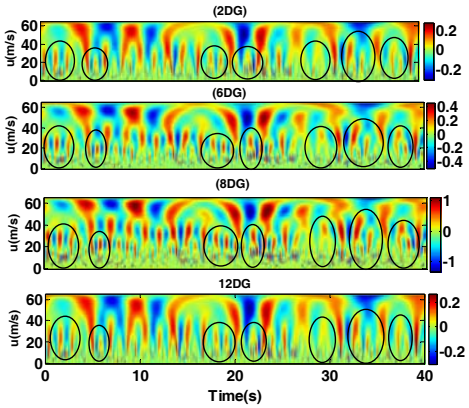

Fig. 6. Comparison of CWT results of the velocity fluctuations at the position (x=2h, y=1.15h) located in the free shear layer using different mother wavelets: 2nd, 6th, 8th and 12th DGW.

It can be seen that the 8th derivative of a Gaussian wavelet (8DGW) can detect well the structures at small and large scales as compared to the other derivative order of the Gaussian.

4.3.1.2 Quantitative Approaches

In order to select the best mother wavelet based on qualitative approach, we use the wavelet entropy measures with different order derivative of the Gaussian applied to the same signals of the velocity fluctuations of turbulent flow located at the section x=2h as shown in Fig. 7.

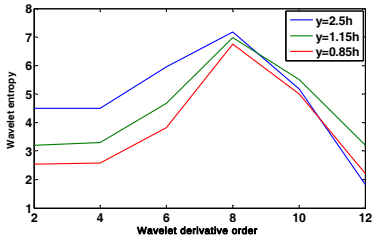

Fig. 7. Wavelet entropy applied to the velocity signals for different positions in the flow at the section x=2h.

We can notice that the 8DGW shows a significantly higher entropy value compared to the other derivative order of the Gaussian.

The results indicate that the 8DGW is the best mother wavelet compared to the other derivative order of the Gaussian for detecting the singularities locations.

The (8DGW) is given by the following expression:

$$\psi(t) = (t^8 - 28t^6 + 210t^4 - 450t^2 + 90)e^{-t^2/2} \quad (16)$$

Its Fourier transform is given by:

$$\hat{\psi}(\omega) = \omega^8 e^{-\frac{\omega^2}{2}} \quad (17)$$

This wavelet has a good localization in time and a poor localization in frequency. Figure 8 depicts the Fourier transform of the 8DGW.

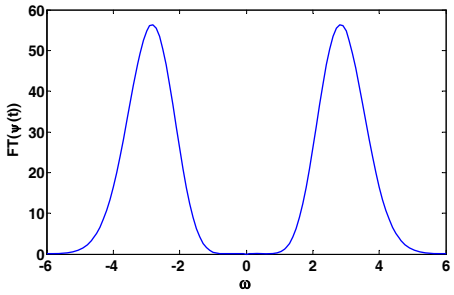

Fig. 8. Fourier transform of the 8DG wavelet.

4.3.2. The Morlet Wavelet

The Morlet wavelet is a complex wavelet function, given by:

$$\psi(t) = \exp(2i\pi\omega_0 t - \frac{t^2}{2}) \quad (18)$$

Its Fourier transform is given by:

$$\hat{\psi}(\omega) = \frac{1}{\sqrt{2\pi}} \exp\left[-\frac{1}{2}(\omega - \omega_0)^2\right] \quad (19)$$

where ω_0 is the non-dimensional central frequency of the mother wavelet.

The Morlet wavelet is a good choice for the CWT, because it contains harmonic components and analogues to the Fourier transform, so it is well localized in term of frequency and has a poor localization in time. Figure 9 shows the Morlet wavelet and its Fourier transform.

5. VISUALIZATION OF MULTISCALE STRUCTURES BY THE CWT

As we have pointed out in the previous section, the turbulent wall jet flow through a backward facing step presents a complex pattern with different regions, where multiscale eddy structures in both space and time are in interaction. The main role of the large energetic eddies due to the external region on reattachment phenomena, is particularly suggested in previous work (Nait Bouda *et al.* 2008). Indeed, the interaction of the large eddies with the separated recirculating zone increases the turbulent diffusion and promotes the flapping of the impingement of the jet on the wall, thus the reattachment length is reduced. In order to better understand the turbulence process in each region over a backward facing step, it is necessary to decompose the turbulent flow into local scales. Consequently, the CWT is the best tool for decomposing and identifying the dynamics of these structures in both space and time. We will here employ the CWT in order to extract instantaneous turbulent structures of different scale eddy structures of the turbulent wall jet flow downstream of the step.

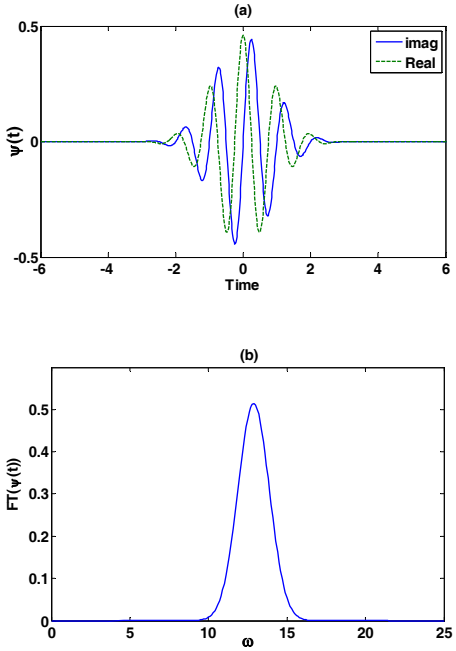

Fig. 9. Morlet wavelet (a) and its Fourier transform (b).

The analysis of the fluctuating velocity signals obtained experimentally downstream of the step is structured in two parts: (1) we analyze the flow structure, at different heights from the wall along the measurement section x=2h, using both the Morlet and The eighth derivative of a Gaussian wavelet. (2) We then apply the CWT using the Morlet wavelet in order to monitor the dragging along of large eddies at different positions downstream of the step.

Since Yule (1978) has shown that, when an eddy passes, the local fluctuating velocity presents large positive and negative peaks, then the flow structure is depicted using the real part of the CWT using both 8DGW and Morlet wavelet. While the modulus of the CWT using the Morlet wavelet is used in order to detect the most representative frequencies, that is, the frequency that contributes most to the total energy of the signal.

The results of the real part of the CWT are displayed on the time-scale and the modulus of the CWT on the time-frequency planes, where the translation parameter b is represented on the abscissa axis (time axis) in both planes, the scale parameter a on the ordinate axis for the time- scale plane and the frequency in the time- frequency plane. The colors indicate the intensities of wavelet coefficients: The red area refers to the maximum values, and the blue area indicates the minimum values. The range of scales between 0 and 65, is chosen arbitrarily to obtain complete picture according to the data (Torrence and Compo 1998).

5.1 Eddy Structure Identification at Along the Measurement Section x=2h

It is known that the Morlet wavelet is well suited to determine locally the frequency of the signal, while the eighth derivative of Gaussian wavelet is more suited for detecting the singularities of the eddy structures. So we use both wavelets here to detect the dominant energetic structures along the measurement section x=2h.

Figure 10 depicts the results of the CWT of the velocity fluctuations at y=2.5h, located in the external region. The real part of the CWT with the Morlet wavelet (Fig. 10(b)) exhibits peaks, alternatively positive and negative, at scale 58, corresponding to the frequency of 1.95Hz. This frequency of large-scale eddies appears as a thin horizontally elongated spot in Fig. 10(c) which represents the modulus of CWT wavelet. On the other hand, the 8DGW helps to localize precisely these energetic structures in time. We refer, for instance, to the presence of verticals patterns oriented at the smaller wavelet scales as shown in Fig. 10(d). For example, eddies with large scale located at 9.5s, 34.5s and 37.5s. These very energetic structures have already been observed at a low frequency in the Fourier spectra (Fig. 4(a)), but were not localized in time. However, the present results have highlighted the existence of large structures in the external region as shown by Nait Bouda *et al.* (2008).

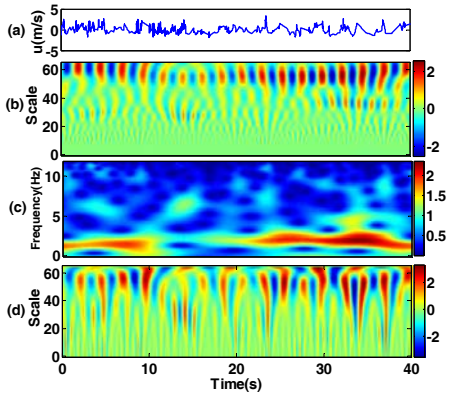

Fig. 10. (a) Instantaneous fluctuating velocity at (x=2h, y=2.5h), (b) the real part of the CWT using the Morlet wavelet, (c) the modulus of the CWT in the time-frequency plane and (d) the real part of the CWT using the 8DGW.

In the shear layer, y=1.15h, the real part of the CWT using the Morlet wavelet exhibits a quasi-periodical peak at different scales (Fig. 11(b)), where the peaks at large scales have a longer duration than the smaller. This result is confirmed with the modulus of CWT wavelet (Fig. 11(c)). In fact, the results show two horizontally elongated spots of 2.1Hz and 3.5Hz with a longer duration than the smaller. On Fig. 11(d), the 8DGW shows the large eddy stretching into small structures. For example, structures with scale 45.49 and 13.75 occur simultaneously at t=22.98s and another stretching structure at 4.9s. The breaking of large structures into small structures was also observable at 7.2s, 9.85s, 11.66s and 27s, indicating the multiscale structures which appear in the shear layer. These results are in accordance with those obtained by Li (1997).

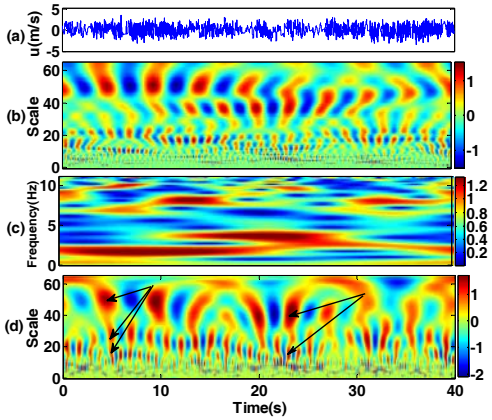

Fig. 11. (a) Instantaneous fluctuating velocity at (x=2h, y=1.15h), (b) the real part of the CWT using the Morlet wavelet, (c) the modulus of the CWT in the time-frequency plane and (d) the real part of the CWT using the 8DGW.

In the recirculation zone, y=0.85h, the real part of the CWT with the Morlet wavelet (Fig. 12(b)) does not show the quasi-periodical comportment at large scales compared to the previous region. We can see the high energy structures with different scales widely spread in the time domain. The large structures are less present and their energy begins to decrease compared to the upper position. But the number of medium and small-scales structures increases. This suggests that the energy transfer begins from large scales (low frequency) to small scales (high-frequency). The modulus of CWT wavelet (Fig. 12 (c)) shows that the energy is distributed between all frequencies and this quite uniformly in space. The 8DGW highlights the process of the structure breakdown at 2s, 16.8s and 23.33s and the stretching of the large eddy into small eddies is also observed at 19.77s and 20.38s, as shown in Fig. 12(d). We can notice also that the 8DGW can't distinguish some peaks at small scales compared to the Morlet wavelet, for example the peaks at small scale with 13 in the range of time between 15s and 25.9s.

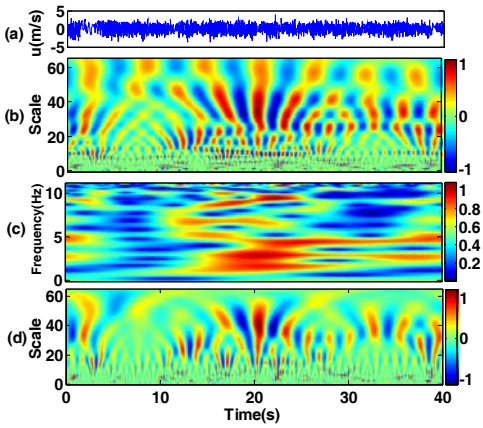

Fig. 12. (a) Instantaneous fluctuating velocity at (x=2h, y=0.85h), (b) the real part of the CWT using the Morlet wavelet, (c) the modulus of the CWT in the time-frequency plane and (d) the real part of the CWT using the 8DGW.

For the region close to the wall, y=0.35h , the real part of the CWT with a Morlet wavelet (Fig. 13(b)) shows that the energy of large scales decreases more as compared to upper positions, indicating that the large eddies are broken down into small eddy structures. It is found also that some peaks are observed at small-scale around frequencies with 5.9 to 7.1Hz as shown in Fig. 13(c), representing the small-scale eddies. The 8DGW (Fig. 13(d)), shows that the number of small scale eddy decreases as compared to the previous regions. This could be due to the viscous dissipative effect near the wall.

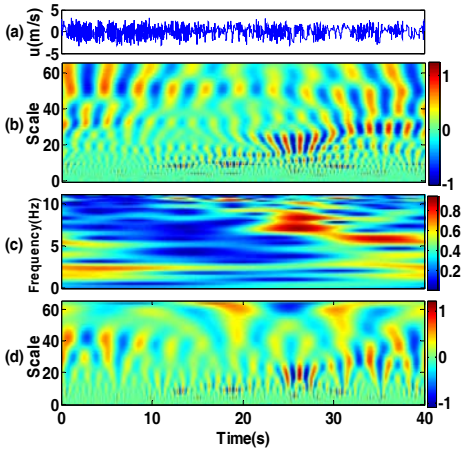

Fig. 13. (a) Instantaneous fluctuating velocity at (x=2h, y=0.35h), (b) the real part of the CWT using the Morlet wavelet, (c) the modulus of the CWT in the time-frequency plane and (d) the real part of the CWT using the 8DGW.

In order to provide a quantitative information about the energy and relative energy (RWE) associated with different scales of these signals, we present in Fig. 14 the wavelet energy spectrum and RWE using Morlet wavelet. From the wavelet energy spectrum (Fig. 14(a)) which is a smoother alternative to the Fourier spectrums that are illustrated in previous section, it is evident that the energy of low frequency (large scale) decreases when approaching the wall. We can notice also that the maximum of energy is reached at low frequencies (large scales), and that this energy is transferred towards the low frequencies in the external region. While for the other regions, we can see the contributions of the medium and high frequencies.

From the Fig. 14(b), we can see that the relative energy gradually increases and converges at scale 58 in the external zone. While the relative energy peaks are widely distributed at various scales in the shear layer, the recirculation zone and in the region close to the wall. In addition, the energy peak in the external zone is higher than it of the other positions and contributing about 45% to the total energy. We can also note that the relative energy decreases at large scale when approaching the wall. These results are in accordance with those obtained by the CWT.

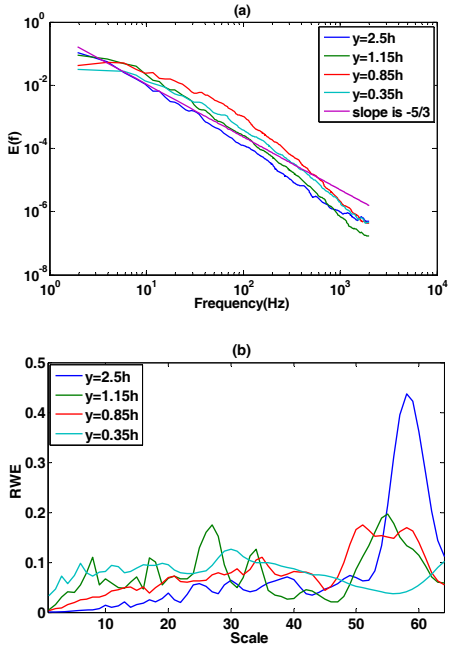

Fig. 14. Wavelet spectrum (a) and the RWE at different position at the section x=2h (b).

The CWT and RWE results show that, the size of eddy structures and their breakup are related to the distance from the wall. In the external region, the high energy is concentrated in the large scale structures which are absolutely evident and contributing about 45% to the total energy. In the shear layer, different scales of structures are observed. The stretching and breakdown of the large eddy into small eddies is also observed. This result is in accordance with those obtained by Li (1997). Additionally, when approaching the wall, it has been found that the energy of large scale structures decreases and their number are reduced, but the number of small scales increases. This

indicates that the large eddy structures are broken into small scale eddy structures for the region close to the wall. It is essentially due to the viscous dissipative effect near the wall.

5.2 Investigation of Large Eddy Structures at Different Regions Downstream of the Step

From this analysis, we would like to monitor the movement, through a backward facing step, of a turbulent structures originating from the external (intermittent) zone of the jet towards reattachment region.

Thus, Figure 15 exhibits the CWT and PSD of the fluctuating velocity in the external region at (x=h, y=3h). We can see, from the Figs (a) and (b), that the maximal energy of eddy structures appears quasi-periodically at the large-scale around 58 corresponding to a frequency about 1.95Hz. The PSD of the signal indicates that the pronounced peak is at the low frequency (large-scale) 1.95Hz (Fig15(c)).

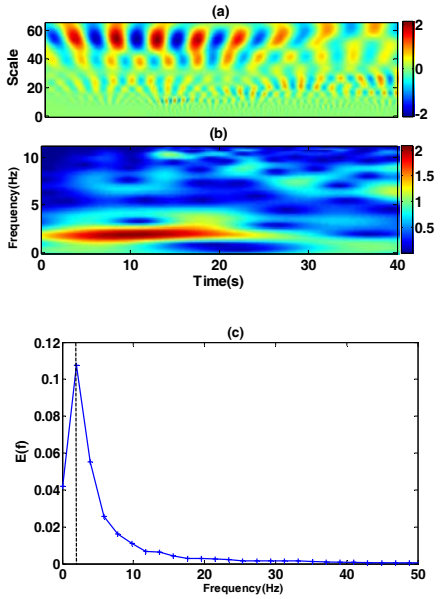

Fig. 15. The real part of the CWT using a Morlet wavelet (a), the modulus of CWT in time frequency plane (b) and the PSD of the fluctuating velocity (c) at (x=h, y=3h) .

The spectral analysis of the signals at the section x=2h, shows that the PSD at y=0.5h (Fig. 16(c)) presents an energy peak at 1.95Hz , corresponding to the frequency of the structures originating from the external zone at x=h; but ends up with less energy. The results of CWT at this position (Fig. 16 (a) and 16(b)) show that the energy of eddy structures at a large scale around 58 corresponding to a frequency about 1.95 Hz decreases as compared to the external region.

The same frequency 1.95Hz is detected at y=0.25h, x=3h. At this position near the wall (Fig. 17), it is obvious to see that, both for the CWT and the PSD, the energy at large scale decreases more than at precedent positions.

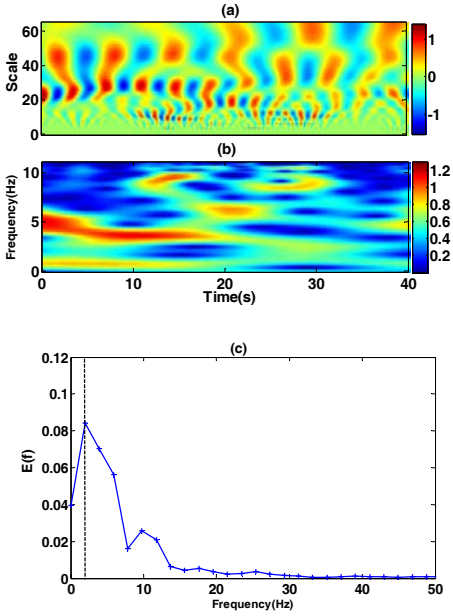

Fig. 16. The real part of the CWT using a Morlet wavelet (a), the modulus of CWT in the time- frequency plane (b) and the PSD of the fluctuating velocity (c) at (x=2h, y=0. 5h).

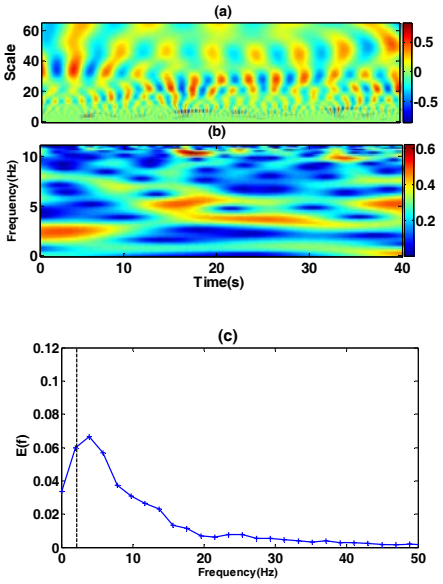

Fig. 17. The real part of the CWT using a Morlet wavelet (a), the modulus of CWT in the time-frequency plane (b) and the PSD of the fluctuating velocity (c) at (x=3h, y=0.25h).

As a validation, the maximal mode of CWT of these signals is shown in Fig. 18. It seems that the maximum energy of the structures and their durations is even lower when approaching the wall.

In the external region (see Fig. 18(a)), the maximal

energy is higher and its duration is longer than at other positions. However, around the recirculation zone (Fig. 18(b)), the maximal energy of eddy structures decreases as compared to the external region. On the other hand, in the region close to the wall (Fig. 18(c)), the maximal energy decreases more and their duration is shorter than at other positions.

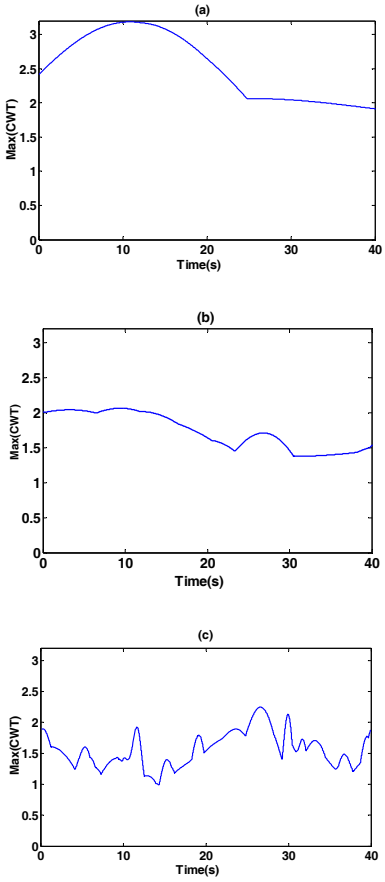

Fig. 18. Maximal mode of CWT at: (a): (x=h, y=3h), (b): (x=2h, y=0. 5h) and (c): (x=3h, x=0.25h).

Figure 19 shows the wavelet spectrum and the RWE of these signals. From the wavelet spectrum (Fig. 19 (a)), we can see that the energy decreases gradually as moving away from the step. Figure 19(b) shows also that the maximum of the RWE is located at the scale 58 in the external region (x=h, y=3h), where the energy contributing about 59% to the total energy, and it decreases gradually along the streamwise direction. These results are in accordance with those obtained by the CWT.

6. CONCLUSIONS

In this study, we have applied the continuous wavelet transform using both a Morlet wavelet and the eighth derivative of a Gaussian wavelet on fluctuating velocity signals obtained experimentally in a turbulent wall jet flow through a backward facing step. We focus our investigation downstream the step where the flow seems to be complex due to the presence of two shear production sources on each side of the maximum velocity line. In particular, the reattachment length in this configuration is found shorter than the case of a usual two-dimensional backward facing step in a channel.

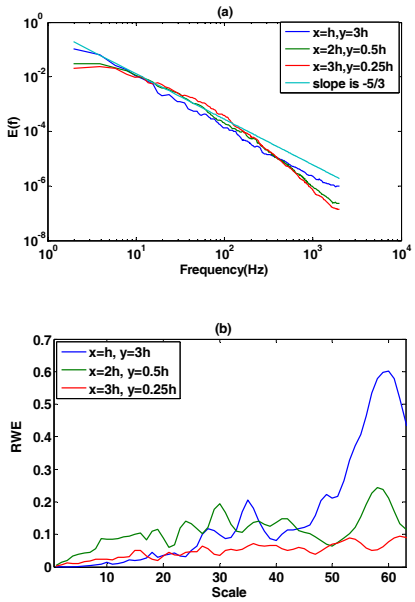

Fig. 19. Wavelet spectrum (a) and the RWE (b) at: (x=h, y=3h), (x=2h, y=0.5h) and (x=3h, y=0.25h).

In the first stage, a Fourier analysis applied to the turbulent velocity fluctuations reveals that the flow loses its equilibrium when approaching the wall. This behavior justifies the presence of multiscale turbulent structures due to the strong interactions between the different zones of the flow. Even if Fourier analysis can represent the energy distribution in the frequency domain, it presents no information on the local structure of the flow, in particular the physical phenomena such as extension of eddies at various scales or their breakups. The main results obtained by the CWT analysis are summarized as follows.

1. The wavelet entropy was used to select an appropriate wavelet mother and 8DGW was selected compared to the wavelets given by other derivative orders of the Gaussian wavelet for detecting the singularities locations.
2. Using the Morlet wavelet, we were able to detect all dominating scales (frequencies). However, in the case of the 8DGW, we could localize the eddy structures at various scales in each region composing the flow downstream a backward facing step.
3. The CWT shows that the size of eddy structures and their breakup are related to the

distance from the wall.

4. The energy of the large eddy structures originating from the wall-jet's external region towards the reattachment region contributing about 59% to the total energy and decreases along their dragging along.

5. This result validates the viewpoint put forward by Nait Bouda *et al*. (2008) where the large structures of the external zone of the wall jet penetrate inwards and generate a high turbulent energy at the wall and introduce a change in the flow dynamics through the backward facing step.

As a perspective, we believe it will be interesting to apply the CWT to investigate other flow configurations where the particle image velocimetry is used.

ACKNOWLEDGEMENTS

We would like to give special thanks to Prof. Jean-Pierre Antoine for his comments which improved the quality of this manuscript. This research work is supported by the Algerian Ministry of Higher Education and Scientific Research. Authors are very grateful to the Algerian Direction Générale de la Recherche Scientifique et du Développement Technologique (DGRSDT) for the financial support.

REFERENCES

Abid, F. and B. Kaffel (2018). Time- frequency wavelet analysis of the interrelationship between the global macro assets and the fear indexes. *Physica A: Statistical Mechanics and its Applications* 490(C), 1028-1045.

Addison, P. S. (2002). *The Illustrated Wavelet Transform Handbook*. Bristol, UK: IOP.

Beibei, X., K. Deming, K. Lingfu, K. Weihang and L. Lie (2018). Analysis of vertical upward oil gas-water three- phase flow based on multiscale time irreversibility. *Flow Measurement and Instrumentation* 62, 9-18.

Belayadi, A., B. Bourahla and F. Mekideche-Chafa (2017). Neurocomputing Techniques to Predict the 2D Structures by Using Lattice Dynamics of Surfaces. *Acta Physica Polonoca A* 132, 1314-1319.

Benedict, L. H., H. Nobach and C. Tropea (1998). Benchmark tests of power spectra from LDA signals, *Proceeding of the 9th International Symposium on Applications of Laser Techniques to Fluid Mechanics*, Lisbon Portugal.

Bernier, D. and K. F. Taylor (1996). Wavelets from square-integrable representations, *SIAM Journal of Mathematical Analysis* 27(2), 594-608.

Coifman, R. R. and M. V. Wickerhauser (1992). Entropy based algorithms for best basis selection. *IEEE Transactions on Information Theory 38 (2), 713– 718.*

Daubechies, I. (1992). Ten lectures on wavelets, SIAM, Philadelphia, PA, Unites States; ISBN: 978-0-89871-274-2.

Daubechies, I., A. Grossmann and Y. Meyer (1986). Painless nonorthogonal expansions. *Journal of Mathematical Physics* 27(5), 1271-1283.

Eriksson, J. G., R.I. Karlsson and J. Persson (1998). An experimental study of a two dimensional plane turbulent wall jet. *Experiments in Fluid* 25, 50-60.

Farge, M. (1992). Wavelet Transforms and their Applications to Turbulence. *Annual Review of Fluid Mechanics* 24, 395-457.

Fernández-Macho, J. (2018). Time- localized wavelet multiple regression and correlation. Physica A: *Statistical Mechanics and its Applications* 492, 1226-1238.

Grossmann, A. and J. Morlet (1984). Decomposition of Hardy Function into Square Integrable Wavelet of Constant Shape. *SIAM Journal on Mathematical Analysis* 15, 723-736.

Grossmann, A. and R. Kronland Martinet (1982). Time and Scale representation obtained through Continuous Wavelet Transform. *In Proceedings of International conference on Applications, Eds.; Elsevier Science Pub*, New-York, pp. 475-482.

Jacob, M. C., A. Louisot, and D. Juvé (2001). Experimental Study of Sound Generated by Backward Facing Steps Under Wall Jet. *AIAA Journal* 39 (7), 1254-1260.

Li, H. (1997). Wavelet auto-correlation analysis applied to eddy structures identification of free turbulent shear flow. *JSME International Journal Series* B 40, 567-576.

Li, H. and T. Nozaki (1995). Wavelet Analysis for the Plane Turbulent Jet. *JSME International Journal Series B 38*, 525-531.

Li, H., M. Takei, M. Ochi, Y. Saito and K. Horii (1999). Application of two-dimensional orthogonal wavelets to multiresolution image analysis of a turbulent jet. *Transactions of the Japan Society for Aeronautical and Space Sciences* 42, 120-127.

Lim, Y. C., F. B. Hsiao, D. B. Wang, C. J. Bai and T. S. Lin (2008). The Study of Coherent Structures in a Sharp-edged Orifice Plane Jet with Wavelet Analysis. *3rd International Symposium on Advanced Fluid/Solid Science and Technology in Experimental Mechanics*, 7-10 Tainan, Taiwan.

Liu, W. and N. Jiang (2004). Three Kinds of Velocity Structure Function in Turbulent Flows. *Chinese Physics Letters* 21 1989-1992.

Lysenko, D. A., I. S. Ertesvag and K. E. Rian (2014). Large-Eddy Simulation of the Flow

Over a Circular Cylinder at Reynolds Number 2.104. *Flow Turbulence Combust* 92, 673- 698.

Meringolo, D. D., A. Colagrossi, S. Marrone and F. Aristodemo (2017). On the filtering of acoustic components in weakly- compressible SPH simulations. *Journal of Fluids and Structures* 70, 1-23.

Monin, A. S. and A. M. Yaglom (1975). Statistical Fluid Mechanics, *Mechanics of Turbulence* 2, MIT Press, Combridge, London.

Nait Bouda, N., A. Babbou and S. Harmand (2014). Reverse flow region associated to a heat transfer in a turbulent wall jet. *International Journal of Thermal Sciences* 85, 151-158.

Nait Bouda, N., R. Schiestel, M. Amielh and C. Rey Benabid, T. (2008). Experimental approach and numerical prediction of a turbulent wall jet over a backward facing step. T. *International Journal of Heat and Fluid Flow* 29, 927-944.

Pope, S. B. (2000). *Turbulent flows*. Cambridge University Press.

Qian, S. (2002). *Introduction to Time-Frequency and Wavelet Transforms*. Prentice Hall PTR: Upper Saddle River. NJ.

Rosso, O. A., S. Blanco, J. Yordanova, V. Kolev., A. Fiqliola, M. Schurmann and E. Basar (2001). Wavelet entropy: a new tool for analysis of short duration brain electrical signals. *Journal of Neuroscience Methods* 105(1), 65–75.

Seena, A. and H. Jin Sung (2011). Wavelet spatial scaling for educing dynamic structures in turbulent open cavity flows. *Journal of Fluids and Structures* 27, 962-975.

Szadkowski, Z. (2014). An Optimization of the FPGA Based Wavelet Trigger in Radio Detection of Cosmic Rays. *IEEE Transactions on Nuclear Science* 62, 993-1001.

Tennekes, H. and J. L. Lumely (1972). *A First Course in Turbulence*. The MIT Press, Cambridge, Massachusetts, and London, England.

Thien, D. N. and S. Harmand (2015). PIV measurements in a turbulent wall jet over a backward-facing step in a three dimensional, non-confined channel. *Flow Measurement and Instrumentation* 42, 26–39.

Torrence, C. and G. P. Compo (1998). A pratical guide to wavelet analysis. *Bulletin of the American Meteorological Society* 79, 61-78.

Watson, J. N. and P. S. Addison (2002). Spectral-temporal filtering of NDT data using wavelet transform modulus maxima. *Mechanics Research Communications* 29, 99-106.

Xia, Z. Y., Y. Tian and N. Jiang (2009). Wavelet spectrum analysis on energy transfer of multi-scale structures in wall turbulence. *Applied Mathematics and Mechanics* 30, 435-443.

Yao, S., Y. Guo, N. Jiang and J. Liu (2015). An experimental study of a turbulent jet impinging on a flat surface. *International Journal of Heat and Mass Transfe* 83, 820–832.

Yule, A. J. (1978). Large –scale structure in mixing layer of a round jet. *Journal of Fluid Mechanics* 89, 413.

Zheng, Y., S. Fujimoto and A. Rinoshika (2016). Combining wavelet transform and POD to analyze wake flow. *Journal of Visualization* 19, 193-210.